Ginu Unnikrishnan
Department of Defense,
Biotechnology High Performance Computing
Software Applications Institute,
Telemedicine and Advanced Technology
Research Center,
United States Army Medical Research and
Development Command,
Fort Detrick, MD 21702;
The Henry M. Jackson Foundation for the
Advancement of Military Medicine, Inc.,
6720A Rockledge Drive,
Bethesda, MD 20817
e-mail: gunnikrishnan@bhsai.org

Haojie Mao
Department of Defense,
Biotechnology High Performance Computing
Software Applications Institute,
Telemedicine and Advanced Technology
Research Center,
United States Army Medical Research and
Development Command,
Fort Detrick, MD 21702;
The Henry M. Jackson Foundation for the
Advancement of Military Medicine, Inc.,
6720A Rockledge Drive,
Bethesda, MD 20817
e-mail: haojie.mao@uwo.ca

Venkata Siva Sai Sujith Sajja
Blast Induced Neurotrauma Division,
Center for Military Psychiatry and
Neurosciences,
Walter Reed Army Institute of Research,
503 Robert Grant Drive,
Silver Spring, MD 20910
e-mail: venkatasivasaisujith.sajja.ctr@mail.mil

Stephen van Albert
Blast Induced Neurotrauma Division,
Center for Military Psychiatry and
Neurosciences,
Walter Reed Army Institute of Research,
503 Robert Grant Drive,
Silver Spring, MD 20910
e-mail: steve.vanalbert@gmail.com

Aravind Sundaramurthy
Department of Defense,
Biotechnology High Performance Computing
Software Applications Institute,
Telemedicine and Advanced Technology
Research Center,
United States Army Medical Research and
Development Command,
Fort Detrick, MD 21702;
The Henry M. Jackson Foundation for the
Advancement of Military Medicine, Inc.,
6720A Rockledge Drive,
Bethesda, MD 20817
e-mail: asundaramurthy@bhsai.org

Animal Orientation Affects Brain Biomechanical Responses to Blast-Wave Exposure

In this study, we investigated how animal orientation within a shock tube influences the biomechanical responses of the brain and cerebral vasculature of a rat when exposed to a blast wave. Using three-dimensional finite element (FE) models, we computed the biomechanical responses when the rat was exposed to the same blast-wave overpressure (100 kPa) in a prone (P), vertical (V), or head-only (HO) orientation. We validated our model by comparing the model-predicted and the experimentally measured brain pressures at the lateral ventricle. For all three orientations, the maximum difference between the predicted and measured pressures was 11%. Animal orientation markedly influenced the predicted peak pressure at the anterior position along the midsagittal plane of the brain (P = 187 kPa; V = 119 kPa; and HO = 142 kPa). However, the relative differences in the predicted peak pressure between the orientations decreased at the medial (21%) and posterior (7%) positions. In contrast to the pressure, the peak strain in the prone orientation relative to the other orientations at the anterior, medial, and posterior positions was 40–88% lower. Similarly, at these positions, the cerebral vasculature strain in the prone orientation was lower than the strain in the other orientations. These results show that animal orientation in a shock tube influences the biomechanical responses of the brain and the cerebral vasculature of the rat, strongly suggesting that a direct comparison of changes in brain tissue observed from animals exposed at different orientations can lead to incorrect conclusions. [DOI: 10.1115/1.4049889]

Keywords: traumatic brain injury, Sprague-Dawley rat, shock tube, advanced blast simulator, finite element model, brain pressure, maximum principal strain

Jose E. Rubio

Department of Defense,
Biotechnology High Performance Computing
Software Applications Institute,
Telemedicine and Advanced Technology
Research Center,
United States Army Medical Research and
Development Command,
Fort Detrick, MD 21702;
The Henry M. Jackson Foundation for the
Advancement of Military Medicine, Inc.,
6720A Rockledge Drive,
Bethesda, MD 20817
e-mail: jrubio@bhsai.org

Dhananjay Radhakrishnan Subramaniam

Department of Defense,
Biotechnology High Performance Computing
Software Applications Institute,
Telemedicine and Advanced Technology
Research Center,
United States Army Medical Research and
Development Command,
Fort Detrick, MD 21702;
The Henry M. Jackson Foundation for the
Advancement of Military Medicine, Inc.,
6720A Rockledge Drive,
Bethesda, MD 20817
e-mail: dsubramaniam@bhsai.org

Joseph Long

Blast Induced Neurotrauma Division,
Center for Military Psychiatry and
Neurosciences,
Walter Reed Army Institute of Research,
503 Robert Grant Drive,
Silver Spring, MD 20910
e-mail: joseph.b.long.civ@mail.mil

Jaques Reifman[1]

Department of Defense,
Biotechnology High Performance Computing
Software Applications Institute,
Telemedicine and Advanced Technology
Research Center,
United States Army Medical Research and
Development Command,
Fort Detrick, MD 21702
e-mail: jaques.reifman.civ@mail.mil

1 Introduction

The inability to directly assess the effects of human exposure to blast waves has led to numerous laboratory studies of animal models in shock tubes [1–15]. In particular, these studies attempt to mimic the interaction between the resulting blast wave from an explosion and the body, which is assumed to cause mild traumatic brain injury (TBI) in humans [16,17]. To this end, a diverse array of experimental setups have been proposed over the years, including those differing in the type of shock tube [12,18–20], animal location within the tube [10,21], and animal orientation with respect to the direction of blast-wave propagation [10,14,19]. These experimental differences make it impractical, if not impossible, to directly compare and contrast cellular and protein-expression changes in brain tissues, and potential brain damage, between studies.

While certain shock tubes, such as the advanced blast simulator (ABS) [8,11,19], and animal locations within them are able to replicate exposure to an idealized Friedlander-type waveform observed in open-field explosions [11,12,21,22], there is no consensus regarding the orientation of the animal with respect to the blast-wave propagation within the tube. For example, for its simplicity and ability to prevent blast waves from causing damage to the animal's lungs [8,20], which is often a major cause of death in shock-tube experiments of rodents [12], the prone orientation, with the head facing the blast wave, is generally chosen [9,12,21]. In contrast, to reduce the interaction of blast waves with the animal's facial structure, such as the snout, the preferred
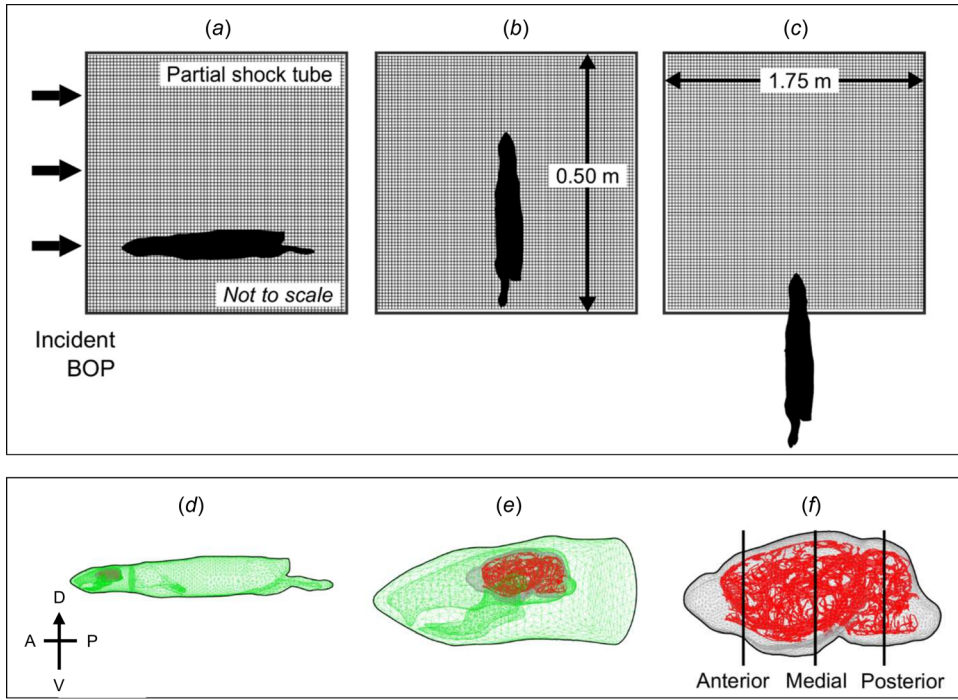
Fig. 1 Representation of the FE mesh of the partial shock tube and the three different body orientations, (a) prone, (b) vertical, and (c) head only, simulated in our study. The bottom panel shows the FE meshes of the rat's (d) body, (e) head, and (f) brain with embedded cerebral vasculature. The three vertical lines in (f) represent the location of the coronal plane at the anterior, medial, and posterior positions. We selected these positions to investigate the effects of body orientation on the biomechanical responses in the brain for a given BOP.

configuration is the side-on orientation [10,18,23,24]. In this orientation, the blast wave impacts the side of the head, preventing any modification of the incoming wave as it reaches the head. Moreover, to evaluate competing theories of blast-induced brain injury [14], animals are often placed in the vertical orientation, with the blast wave facing the ventral surface and interacting with either the entire body (henceforth referred to as the vertical orientation), only the head (the head-only orientation), or only the torso [7,11,14,19].

Despite these differences in animal orientation, alterations in brain tissue observed in one orientation are often compared to those in a different orientation [7,12,19,25–27], without consideration of the effects of differences in brain morphology and angle of incidence of the blast wave at different orientations. Indeed, animal orientation inside a shock tube influences the functional behavior [1] and expression levels of proteins [8] in the rat brain, even when the blast overpressure (BOP) is identical. This effect of animal orientation on functional behavior and protein expression is believed to result from variations in the biomechanical responses of the brain, such as stress and strain, due to the different orientations [1,8,9]. Hence, a systematic characterization of such biomechanical responses would help us to determine when and whether such comparisons are appropriate and allow us to link predictions of brain stress and strain levels with experimental observations of brain-tissue alterations to establish injury thresholds.

In this study, we characterized the biomechanical responses throughout the brain and cerebral vasculature of a rat exposed to the same blast wave in a shock tube at three different orientations: prone, vertical, and head only. We used a previously developed three-dimensional (3D) high-fidelity finite element (FE) model of a rat head [28] to predict these biomechanical responses and validated the model predictions by performing experiments on adult male Sprague-Dawley rats using the ABS for each of the three orientations. We characterized how the animal orientation with respect to the direction of blast-wave propagation in a shock tube

influences the biomechanical responses of the brain, when the animal is subjected to an identical blast wave.

2 Materials and Methods

2.1 Three-Dimensional Finite Element Model of a Rat. *Geometry and finite element mesh*: We previously developed and validated a 3D high-fidelity FE model of a rat head to simulate blast exposure in a shock tube [28]. The FE model consists of the face (including the scalp and musculature), skull (including the facial bones), brain, and cerebral vasculature. Here, we extended our rat-head model to include the torso of the animal (including the forearm and hindlimbs). However, to reduce the computational time to run simulations of the FE model, we did not represent the internal organs in the torso, for example, the vertebrae, ribs, or heart.

We obtained the geometry of the rat's body from the anatomical representation developed at Duke University [29]. Previously, we used this representation to develop the FE model of the rat head [28] and to simulate whole-body thermoregulatory responses to environmental and exertional heat stressors [30,31]. After integrating the geometry of the rat torso with our previously developed rat-head geometry, we meshed the face, skull, brain, and torso using 268,741 quadratic (ten-noded), tetrahedral elements of type C3D10M (Fig. 1), using ABAQUS v6.17 (Dassault Systèmes, Vélizy-Villacoublay, France). The FE mesh consisted of elements having an average minimum edge length of 0.61 mm for the face, 0.32 mm for the skull, 0.24 mm for the brain, and 1.71 mm for the torso (Figs. 1(d)–1(f)). Because here we used the same FE mesh size as in our previous work for the rat brain, we did not re-do a mesh convergence study [28].

For the skull, brain, and cerebral vasculature, we used the same mesh parameters as in our previous FE model [28]. Briefly, the skull (including the facial bones) and brain consisted of 55,169 and 133,853 quadratic elements (C3D10M), respectively, where

Components	Density (kg/m^3)	Hyperelastic constants			Viscous constants	
		Bulk modulus (GPa)	Shear modulus (kPa)	α	Relaxation modulus ratio	Decay constant (s^{-1})
Cerebrum	1040	2.0	11.9	6.5	0.103	990
Cerebellum	1040	2.0	8.3	8.2	0.274	402
Brainstem	1040	2.0	12.3	4.7	0.112	1081

α—material constant.

we further subdivided the brain into three distinct regions, the cerebrum, cerebellum, and brainstem. We created the geometry of the cerebral vasculature from microcomputed tomography images and then used Hypermesh 2017.1 (Altair Engineering, Troy, MI) to mesh the geometry with 316,182 linear, triangular shell elements (S3) having an average minimum edge length of 0.07 mm. In addition, we considered the cerebral vasculature as a network of hollow pipes without any blood flow with a thickness of 0.01 mm and having a total volume of 115.76 mm^3. Finally, we coupled the tetrahedral elements of the brain and the triangular elements of the vasculature using the embedding-element technique in ABAQUS.

Material properties: We represented the tissues of the brain (i.e., the cerebrum, cerebellum, and brainstem) as nearly incompressible (bulk modulus = 2.0 GPa), hyper-viscoelastic materials, using a one-term Ogden model with a one-term Prony-series [28]. We obtained the material properties for the brain (Table 1) from high-strain-rate shear tests performed on tissues from the cerebrum, cerebellum, and brainstem of male Sprague-Dawley rats [32]. We represented the cerebral vasculature as a nearly incompressible, hyperelastic material, using a one-term Ogden model with a shear modulus of 0.63 MPa (α = 4.3) obtained from high-strain-rate axial tests of the middle cerebral arteries in male Sprague-Dawley rats [33]. We represented the face as a nearly incompressible, hyperelastic material using a one-term Ogden model with a shear modulus of 75.00 MPa (α = 15.0). Similarly, the torso was considered as a nearly incompressible, hyperelastic material with a shear modulus of 1.25 MPa (α = 3.0). We modeled the skull as a compressible (Poisson's ratio = 0.33), linear elastic material with an elastic modulus of 1.00 GPa.

2.2   Three-Dimensional Finite Element Model of a Shock Tube. Using ABAQUS, we created the geometry of a 3D partial shock tube with a 0.50×0.50 m^2 cross-sectional area and 1.75 m in length (Figs. 1(a)–1(c)). We meshed the shock tube using approximately 0.9×10^6 Eulerian (EC3D8R) elements and assigned the properties of an ideal gas (density = 1.23 kg m^{-3}; specific gas constant = 287 J kg^{-1} K^{-1}, and initial temperature = 300 K) to the air in the shock tube. The FE mesh representing the shock tube had an average minimum edge length of 4 mm. As in previous studies [21,28,34], we set the air velocity perpendicular to the shock-tube walls to zero, which allowed an incident blast wave provided at the inlet surface of the tube to propagate along the incident direction as a planar blast wave. We set the time profile of the incident BOP as the pressure boundary condition at the inlet surface of the partial shock tube (Fig. 2), while not assigning any boundary condition to the outlet surface. We performed all simulations using ABAQUS v6.17.

2.3   Blast Simulation. We used the Eulerian–Lagrangian technique in ABAQUS to couple the shock-tube FE model with the FE model of the rat. We used a penalty contact algorithm with frictionless tangential-sliding behavior and hard-contact normal behavior to couple the shock-tube elements with the FE model of the rat body. With the animal placed at a distance of 0.20 m from the inlet surface of the partial shock tube, we performed simulations of a single blast exposure at an incident BOP of 100 kPa
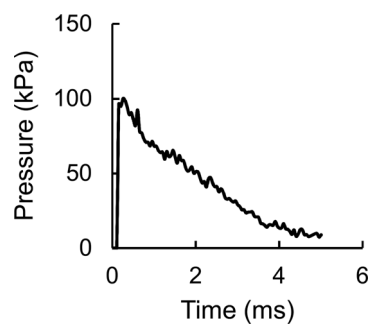

Fig. 2   Time profile of the 100 kPa incident blast overpressure used as an input at the inlet surface of the partial shock tube

for three different orientations: prone, vertical, and head-only (Fig. 1). In the prone orientation, we aligned the anterior–posterior axis of the rat in the direction of the blast-wave propagation, with the head facing the blast wave (Fig. 1(a)). In the vertical orientation, we aligned the anterior–posterior axis perpendicular to the direction of the blast-wave propagation, with the ventral surface of the animal facing the blast wave (Fig. 1(b)). In the head-only orientation, we positioned the rat vertically but with only the head of the animal placed inside the shock tube (Fig. 1(c)). For all three orientations, the animal was not constrained in any direction.

Using the blast simulations, we quantified the effects of animal orientation on the biomechanical responses (i.e., pressure, von Mises stress, maximum principal strain, and strain rate) in the brain of a rat and assessed the maximum principal strain of the brain's cerebral vasculature.

2.4   Experimental Setup. To validate our computational models, we performed shock-tube experiments on 10- to 12-week old (330 to 360 g) male Sprague-Dawley rats (Charles River Laboratories, Wilmington, MA), using an ABS located at the Walter Reed Army Institute of Research (WRAIR, Silver Spring, MD). The ABS is a compressed-gas shock tube with a 0.15 m-long compression section and a 6.40-m-long transition/expansion test section [2,8] with a 0.61×0.61 m^2 cross-sectional area with an end wave eliminator. The Institutional Animal Care and Use Committees at WRAIR, as well as the Animal Care and Use Review Office of the U.S. Army Medical Research and Development Command, Ft. Detrick, MD, approved all experimental protocols. We conducted all animal experiments in a facility accredited by The Association for Assessment and Accreditation of Laboratory Animal Care International (AAALACi), in compliance with the Animal Welfare Act and other federal statutes and regulations relating to animals and experiments involving animals, and adhered to principles stated in the Guide for the Care and Use of Laboratory Animals published by the National Research Council (NRC), 2011 edition.

We placed each isoflurane-anesthetized animal in the shock tube (at a distance of 2.83 m from the compression chamber) and exposed it to a single BOP wave of 100 kPa in the prone, vertical, or head-only orientation ($n = 4$ animals per orientation). In the
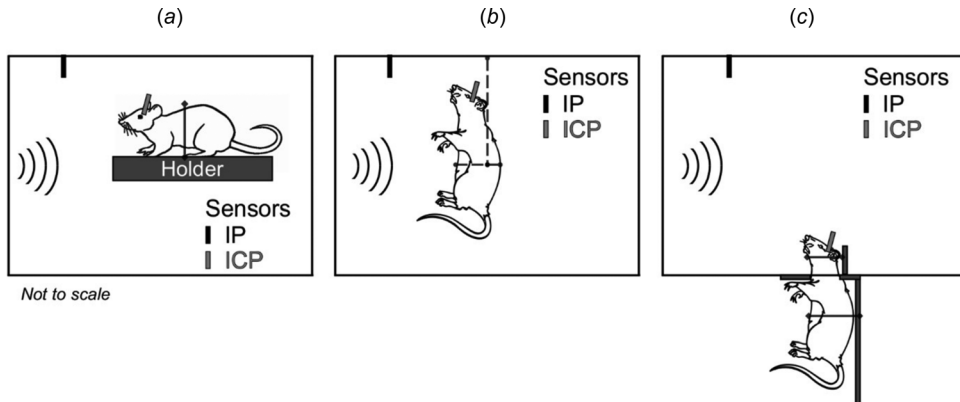
Fig. 3 Schematic representation of the animal setup inside the shock tube. (*a*) Prone: animal positioned in a horizontal orientation with its head facing the oncoming blast wave. In this setup, the ventral surface of the animal rested on top of an aluminum holder, with the animal tightly secured to the holder by a plastic net. (*b*) Vertical: animal positioned in a vertical orientation with its ventral surface facing the oncoming blast wave. We mounted the animal in a custom-made sling inside the test section of the shock tube. (*c*) Head only: animal positioned in a vertical orientation facing the oncoming blast wave, with only the head protruding into the test section of the shock tube though a fitted opening at the bottom wall. Additionally, we wrapped flexible strings around the head and attached them to two vertical pins to keep the head in a vertical orientation while minimally constraining its motion. For all experiments, we measured the incident pressure (IP) and the intracranial pressure (ICP).

prone orientation (Fig. 3(*a*)), we strapped the animal to a raised aluminum holder using a plastic net, with the animal's head facing the blast wave [8]. In the vertical orientation (Fig. 3(*b*)), we suspended the animal from overhead rails inside of the shock tube, using a custom-made sling with the ventral surface of the animal facing the blast wave. In the prone and vertical orientations, we exposed the whole body of the animal to the blast wave. In the head-only orientation (Fig. 3(*c*)), we used a fixture to hold the head into the shock tube through an opening at the bottom wall of the tube. Additionally, we wrapped flexible strings around the head and attached them to two vertical pins to keep the head in a vertical orientation while minimally constraining its motion. We exposed the ventral surface of the head to the blast wave, whereas we positioned the torso outside of the shock tube to shield it from the blast wave.

During the experiments, we measured the time profile of the static pressure in the shock tube using a custom-designed pitot-tube sensor (model 8515C-50; Meggitt Sensing Systems, Irvine, CA). We measured the brain pressure by surgically inserting a Millar pressure-catheter sensor (Model SPR-407; ADInstruments, Colorado Springs, CO) into the lateral ventricle. To implant the brain pressure sensor, we anesthetized the animals using isoflurane. Next, we incised a small section of the scalp to expose the skull. Then, we drilled a small hole (2 mm diameter) in the right frontal bone (-1.40 mm relative to Bregma) and slowly inserted a sterilized stainless steel guide cannula (18 gauge, 10 mm long) into the brain to a depth of 3–4 mm until the tip of the cannula reached the right lateral ventricle. Following, we anchored the cannula to the frontal bone using dental cement and proceeded to close the wound. Finally, we inserted a miniature Millar pressure-catheter sensor (Model SPR-407, AD Instruments) into the cannula. After implanting the sensor, we secured the animal to the corresponding setup and monitored the signal for 10 min. We recorded the data at a sampling frequency of 0.8 MHz using a data recorder (Model TMX-18; Astro-Nova, Inc., West Warwick, RI).

3 Results

3.1 Blast-Wave Dynamics. We compared the spatial evolution of air pressure predicted by the coupled FE model for each of the three orientations (Figs. 4(*a*)–4(*c*)). In the prone orientation, the maximum reflected pressure occurred at the tip of the nose, as

reported previously [28,34]. As expected, the reflected pressure was concentrated in front of the torso in the vertical orientation, and near the bottom wall of the shock tube in front of the head in the head-only orientation. For the prone orientation, the incoming blast wave reflected from the nose and traversed the dorsal and ventral surfaces of the animal with equal intensity (Fig. 4(*a*)). In contrast, for the vertical and head-only orientations (Figs. 4(*b*) and 4(*c*), respectively), the blast wave reflected from the ventral side of the head, causing a higher pressure on its surface when compared to the dorsal surface. Moreover, for the vertical orientation, when compared to the head-only orientation, the interaction of the blast wave with the torso induced a higher reflected pressure. At an incident BOP of 100 kPa, the maximum reflected pressure in the prone orientation was 130 kPa, which was smaller than that in the vertical orientation (194 kPa) and the head-only orientation (178 kPa).

3.2 Brain Pressure, Von Mises Stress, Maximum Principal Strain, and Strain Rate. From the FE simulations, we determined the biomechanical responses (i.e., pressure, von Mises stress, and maximum principal strain) of the rat brain for each of the three orientations. Then, we validated our model by comparing the experimentally measured brain pressures at the ventricle with the model predictions. The temporal profiles of the model-predicted and the experimentally measured brain pressures were similar to the temporal profile of the incident blast pressure (Figs. 5(*a*)–5(*c*) and 2). For each of the three orientations, the predicted and measured pressure profiles were in close agreement, with relatively small differences in peak pressure for the prone (10.3%), vertical (3.6%), and head-only (2.4%) orientations. For the vertical (Fig. 5(*b*)) and head-only (Fig. 5(*c*)) orientations, oscillations in the predicted pressure throughout the profile were higher than those in the prone orientation (Fig. 5(*a*)).

Pressure propagation in the brain depended on the orientation of the animal with respect to the direction of the blast-wave propagation (Fig. 6). In the prone orientation, the blast wave propagated from the anterior to the posterior region of the brain (Fig. 6(*a*)), while for the vertical and head-only orientations, it propagated from the ventral to the dorsal region of the brain (Figs. 6(*b*) and 6(*c*)). In the prone and vertical orientations, the brain pressure initially ($t = 0.88$ ms) propagated in a relatively straight line, unlike the somewhat curvilinear pressure propagation in the head-only orientation. In contrast to brain pressure, at all orientations, the
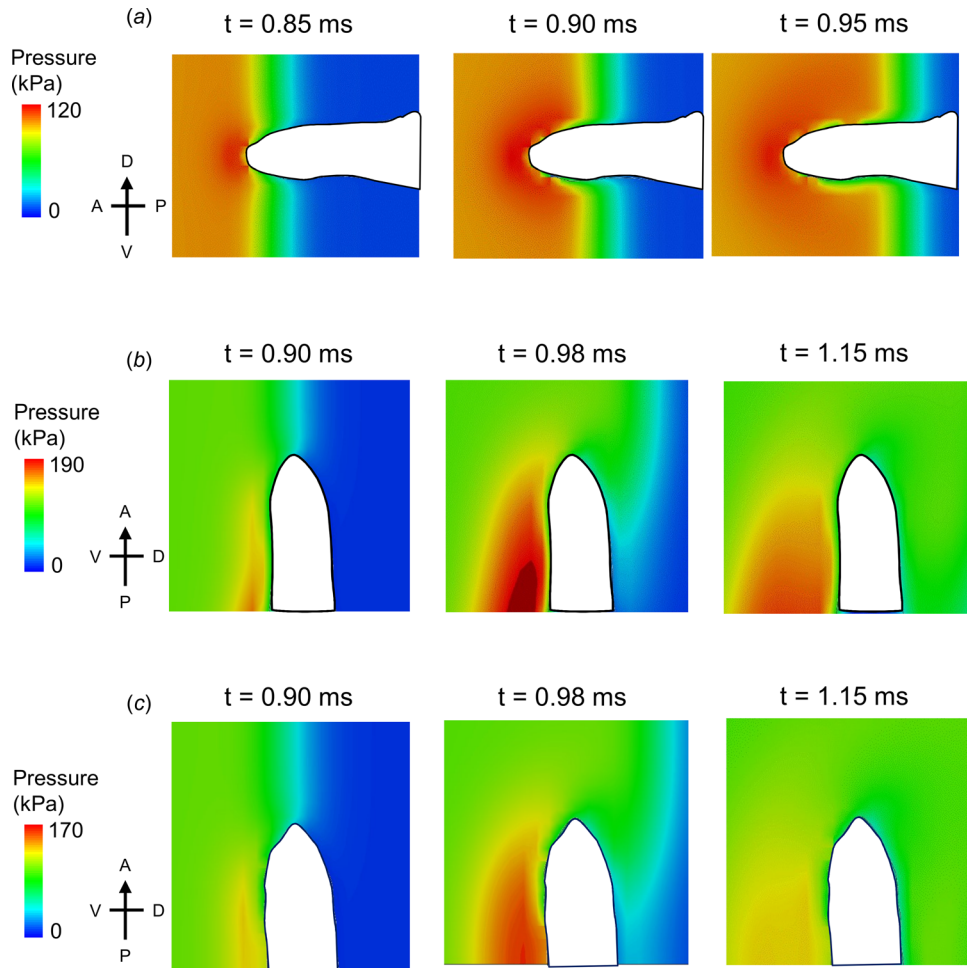
Fig. 4 Temporal and spatial propagation of the air pressure near the rat head in a shock tube in the (*a*) prone, (*b*) vertical, and (*c*) head-only orientations
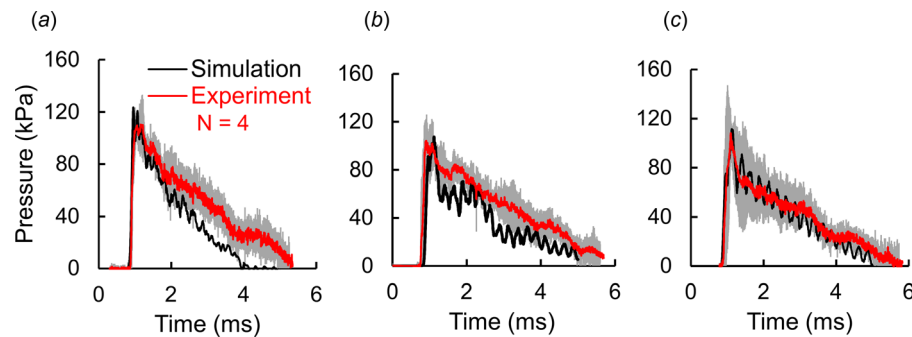

Fig. 5 Comparison of brain pressures predicted by the finite element models (black lines) with the experimental data (gray lines and shaded regions; mean ± two standard errors of the mean)

von Mises stress initially developed at the peripheral regions of the brain (Fig. 7) and propagated inwards toward the center of the brain as time progressed. The magnitude of the von Mises stress in the prone orientation (Fig. 7(*a*), reduced scale from 0 to 1 kPa) was lower than that in the vertical or head-only orientations (Figs. 7(*b*) and 7(*c*)).

To further investigate the effect of animal orientation on the brain pressure, we determined the peak brain pressure at the anterior, medial, and posterior positions on the midsagittal plane of the rat brain. The peak pressure was highest in the prone orientation at the anterior and medial positions (Fig. 8(*a*)). Specifically,

the peak pressure in the prone orientation was greater than the peak pressures in the vertical and head-only orientations by 57 and 37%, respectively, at the anterior position, and by 21 and 12%, respectively, at the medial position. In contrast, at the posterior position, the peak pressure in the prone orientation was higher than that in the head-only orientation by 7% but was also lower than that in the vertical orientation by 7%. In addition, we also observed a similar variation in the peak and 90th percentile biomechanical responses on the coronal plane at the anterior, medial, and posterior positions (Table 2). Interestingly, the predicted strain rate for the vertical orientation was considerably higher
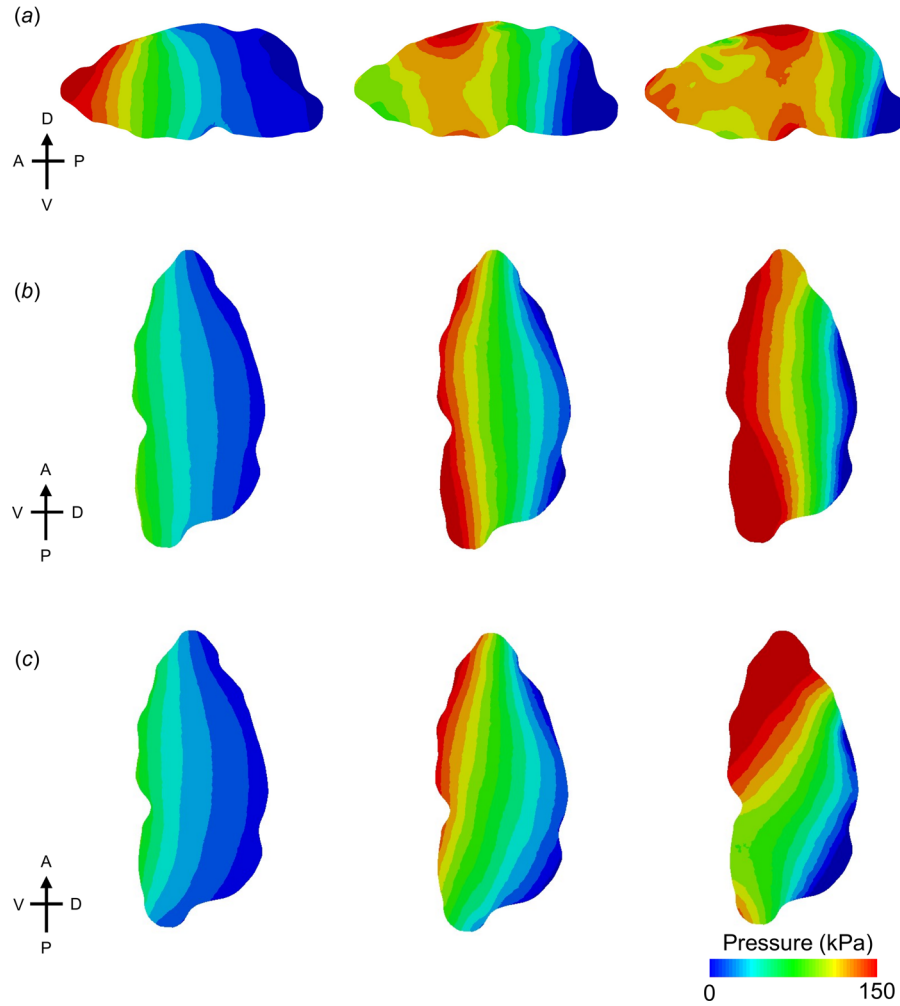
Fig. 6 Temporal and spatial propagation of the brain pressure along the midsagittal plane of the rat brain in the (*a*) prone, (*b*) vertical, and (*c*) head-only orientations. A—anterior; D—dorsal; P—posterior; V—ventral.

than that for the prone orientation by as much as 68%. In the medial coronal plane, the peak brain pressure for the vertical and head-only orientations was concentrated at the ventral surface, while for the prone orientation the peak pressure was mostly manifested at the dorsal surface (Fig. 9(*a*)).

In contrast to peak brain pressure, the peak of the maximum principal strain predicted by the FE model in the prone orientation was considerably smaller than that in the vertical or head-only orientation at each of the three positions (Fig. 8(*b*)). Relative to the other orientations, the peak strain in the prone orientation was lower by 43–70% at the anterior position, 73–88% at the medial position, and 40–80% at the posterior position. We also observed considerable differences in the predicted peak strain for the three orientations at the medial coronal plane (Fig. 9(*b*)). Similarly, the displacement of the nose tip in the prone orientation (2 mm) was considerably smaller than that in the vertical orientation (10 mm) and the head-only orientation (7 mm).

3.3 Maximum Principal Strain of the Cerebral Vasculature. We also determined the maximum principal strain of the cerebral vasculature at three similar positions (i.e., anterior, medial, and posterior) for each of the three orientations (Fig. 10). As was the case for brain strain, the maximum principal strain of the cerebral

vasculature was considerably higher in the vertical orientation (Fig. 10(*b*)) than in the prone (Fig. 10(*a*)) or head-only (Fig. 10(*c*)) orientations. However, in contrast to the brain pressure, the strain of the cerebral vasculature developed slowly and later in the simulation, consistent with our previous observation [28].

4 Discussion

Using a 3D FE model of a rat head and torso, we systematically evaluated the influence of animal orientation on the biomechanical responses of brain tissues and cerebral vasculature during exposure to a blast wave in a shock tube. Specifically, we extended our previously developed model of a rat head [28] consisting of the face, skull, brain, and cerebral vasculature, by coupling a model of the rat torso to the head. Then, we used the enhanced model to determine the responses of the brain to blast-wave exposures in the prone, vertical, and head-only orientations. We examined the prone orientation, because it is the most widely used orientation for blast-exposure studies in a shock tube [4,5,9,12,21], as well as the head-only [11,19] and vertical orientations [14], which have been used to determine the contributions of the direct mechanisms (characterized by blast-wave exposure to the head) and the indirect mechanisms (characterized by blast-wave exposure to the torso) as potential pathways to blast-induced
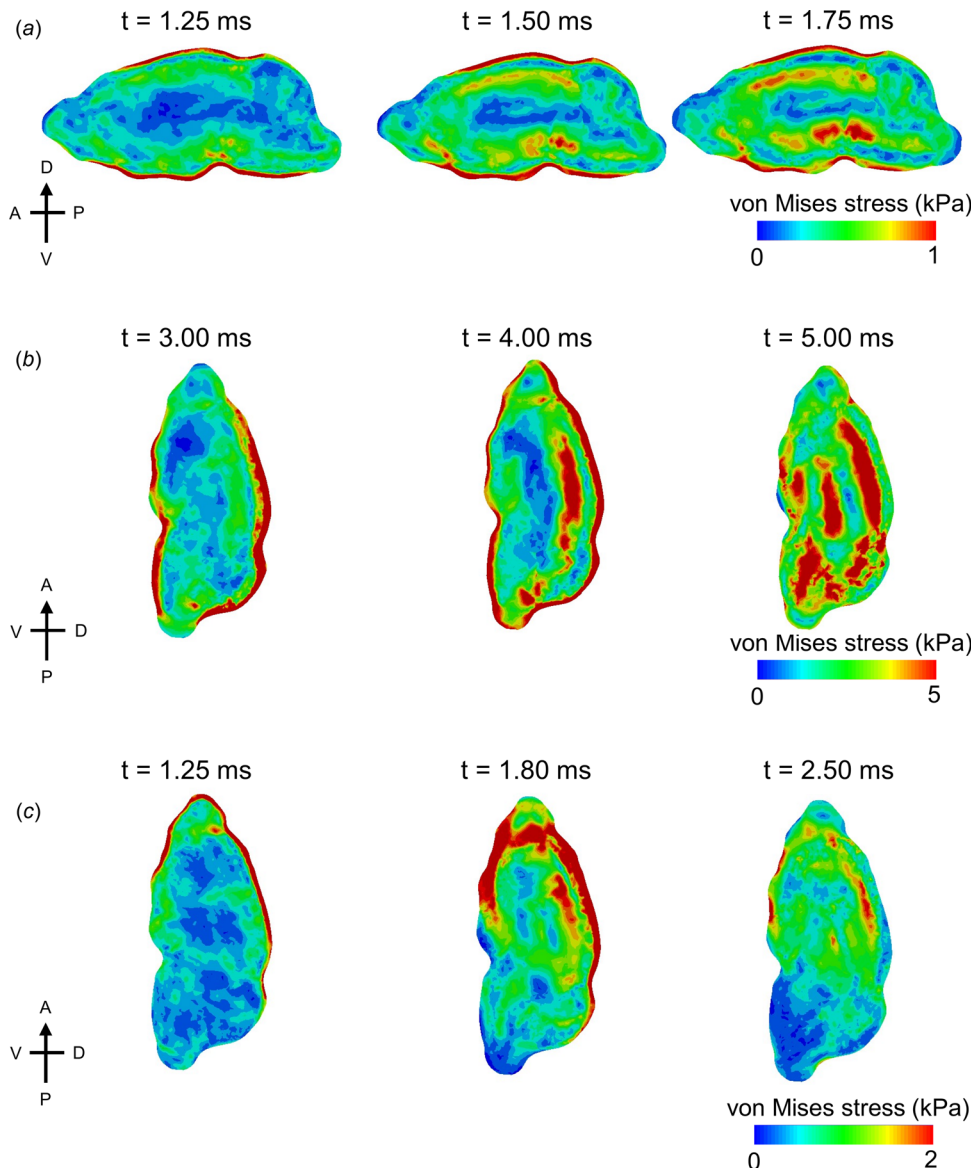
Fig. 7 Temporal and spatial propagation of the von Mises stress along the midsagittal plane of a rat brain in the (*a*) prone, (*b*) vertical, and (*c*) head-only orientations. A—anterior; D—dorsal; P—posterior; V—ventral.
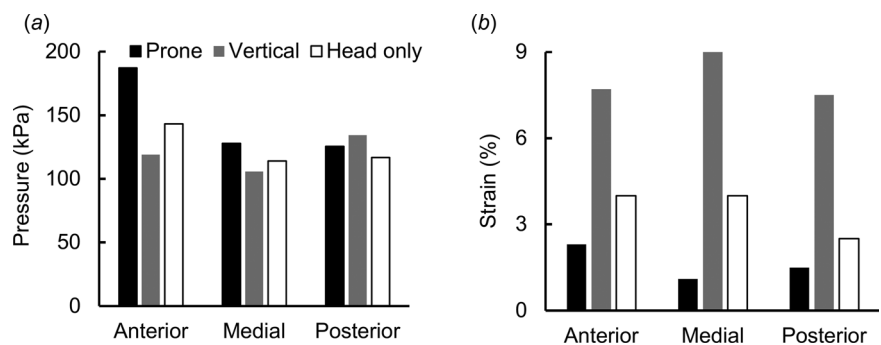

Fig. 8 (*a*) Peak brain pressure and (*b*) peak of the maximum principal strain at the anterior, medial, and posterior positions on the midsagittal plane of a rat brain when the animal was exposed to a 100 kPa blast wave in the prone, vertical, and head-only orientations

Table 2 Peak and 90th percentile biomechanical responses computed in the coronal plane at the anterior, medial, and lateral positions for simulations of blast-wave exposures in the prone, vertical, and head-only orientations

| Parameter	Anterior		Medial		Posterior	
	Maximum	90th percentile	Maximum	90th percentile	Maximum	90th percentile
Brain pressure (kPa)						
Prone	232.91	222.69	217.90	163.40	221.95	161.83
Vertical	183.68	155.79	216.08	175.75	220.66	184.96
Head only	212.47	186.01	200.74	166.03	186.21	141.54
Brain strain (%)						
Prone	6.41	2.73	7.74	4.14	5.79	2.92
Vertical	31.89	19.71	29.69	19.36	25.68	19.78
Head only	21.28	11.57	14.20	7.69	11.19	5.19
Vasculature strain (%)						
Prone	2.27	1.18	3.50	1.42	1.91	1.04
Vertical	17.19	8.55	17.02	9.49	18.60	9.10
Head only	7.72	3.95	7.95	3.52	3.48	1.73
Brain strain rate (s^{-1})						
Prone	266.14	124.43	428.07	163.88	522.05	188.19
Vertical	719.10	391.85	824.33	466.07	748.88	489.35
Head only	528.56	312.26	513.88	226.65	417.68	174.84
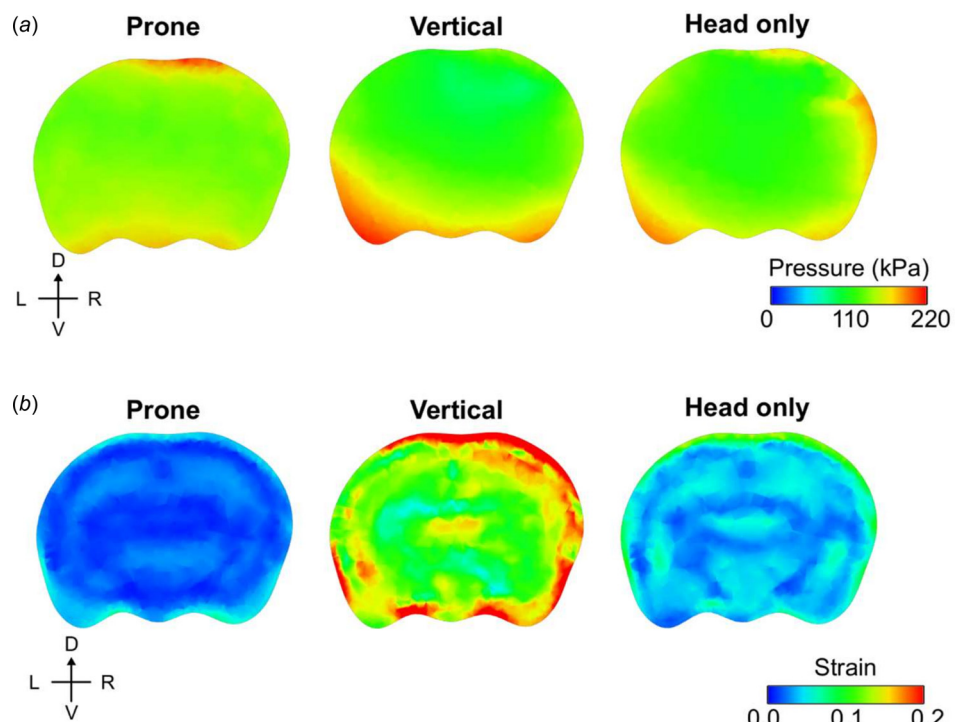
Fig. 9 (a) Peak brain pressure and (b) peak of the maximum principal strain at the coronal plane in the medial position of a rat brain when the animal was exposed to a 100 kPa blast wave in the prone, vertical, and head-only orientations

TBI. We validated our FE model for each of the three orientations by comparing the FE predictions of the temporal pressure profile at the lateral ventricle of the rat brain with experimentally measured values for an incident BOP of 100 kPa.

Our study showed that the orientation of the animal influenced not only the blast-wave dynamics in the shock tube (Fig. 4), but also the biomechanical responses of the brain (Figs. 5–9) and the cerebral vasculature (Fig. 10). In all orientations, the maximum reflected pressure occurred near the body. This amplification, which occurs as the air molecules of the blast wave are brought to rest abruptly and further compressed, depends on the incident

BOP, the geometry and material properties of the exposed object, and the angle of incidence of the blast-wave impact. The amplification in the vertical orientation was considerably higher than that in both the prone and head-only orientations, as the surface area of the animal exposed to the blast wave, specifically in the direction of blast-wave propagation, was greatest in the vertical orientation (Fig. 4). The prone orientation, which offers the least resistance to the propagation of the wave, resulted in the lowest reflected pressure (Fig. 4(a)), the smallest animal displacement, and a temporal pressure profile smoother than that of both the vertical and head-only orientations (Fig. 5). Despite these
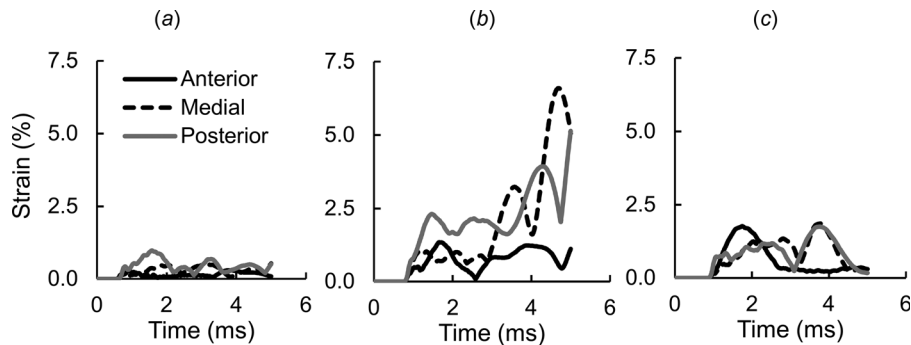
Fig. 10 Temporal evolution of the maximum principal strain of the cerebral vasculature at the anterior, medial, and posterior positions on the midsagittal plane of a rat brain in the (*a*) prone, (*b*) vertical, and (*c*) head-only orientations, for a 100 kPa blast-wave exposure

oscillations, the pressure profile tracked the incident pressure profile in the vertical and head-only orientations, as it did in the prone orientation [21].

Propagation of the pressure wave in the brain followed the direction of the blast wave along the length of the shock tube in the prone orientation (i.e., from the anterior to the posterior direction) and in the vertical and head-only orientations (i.e., from the ventral to the dorsal direction). The pressure along the midsagittal plane of the brain in the prone orientation was greatest at the anterior position and decreased by 33% as the pressure wave reached the posterior position (Fig. 8(*a*)). Moreover, the brain pressure for each of the three orientations (Fig. 6) followed a pattern that was similar to that of the reflected air pressure in the shock tube (Fig. 4). For example, for the prone orientation, the dorsal and ventral regions of the brain were subjected to pressures of equal intensity (Fig. 6(*a*)), similar to those observed for the air pressure (Fig. 4(*a*)). However, as expected, for the vertical orientation, the ventral surface of the brain was subjected to a higher pressure than the dorsal surface (Fig. 6(*b*)), in line with the reflected pressure around the rat head in the shock tube for this orientation (Fig. 4(*b*)). For the prone and vertical orientations, the pressure propagated along a vertical plane (Figs. 6(*a*) and 6(*b*)). In contrast, it propagated in a curvilinear fashion in the head-only orientation (Fig. 6(*c*)), because the proximity of the head to the bottom wall of the shock tube shielded the head against pressure transmission into the brain. This shielding effect is responsible for the nearly identical peak brain pressures at the medial and posterior positions in the rat brain for the head-only orientation (Fig. 8(*a*), center and right white bars). In the vertical orientation, however, where this shielding effect was absent, the peak pressure at the posterior position was higher than that at the medial position (Fig. 8(*a*), right and center gray bars).

The differences in the predicted brain pressures between orientations decreased from the anterior to the posterior position. For example, at the anterior position, the difference in pressure between the prone and vertical (head-only) orientations was 57 (37)%, which decreased to 21 (12)% at the medial position and to 7 (7)% at the posterior position. The measured peak pressures at the ventricle showed only minor differences between the three orientations. The average (standard deviation) peak pressures in the prone, vertical, and head-only orientations were 118.8 (8.4), 115.3 (8.5), and 118.0 (8.9) kPa, respectively. Interestingly, when compared with animals exposed to frontal blasts, previous studies have reported a significant reduction of brain pressure in animals exposed to side-on blasts [5,9]. The results from our simulations suggest that this reduction could be due to the placement of the sensor away from the initial point of contact with the blast wave. Indeed, in the study by Leonardi et al. [9] using rats, the sensor was placed on the right side of the head in alignment with the para-sagittal plane, while the shock wave made initial contact with the left side.

In contrast to brain pressure, the von Mises stress in the prone, vertical, and head-only orientations developed after the initial blast wave had passed through the brain. At first, it was concentrated in the peripheral regions of the brain (i.e., near the skull), and then it propagated deep into the brain with time (Fig. 7), consistent with prior studies on blast exposure in the prone orientation [21,28]. The von Mises stress in the vertical orientation was greater than the stress in both the prone and head-only orientations, possibly because of head movement or skull deformation during blast exposure [3,35,36]. The maximum principal strain in the brain was influenced similarly by the orientation of the animal. The strain was greatest in the vertical orientation (Figs. 8(*b*) and 9(*b*)), as the dynamic force acting on the animal body in this orientation was larger than it was in both the prone and head-only orientations. Similarly, the cerebral vasculature strain in the vertical orientation was considerably larger than that in both the prone and head-only orientations (Fig. 10).

Our study shows that neither measurements of pressure at the ventricle nor predictions of pressure at the medial and posterior positions on the midsagittal plane of the brain alone can by themselves capture the effects of animal orientation. By varying the animal orientation, we identified differences in (1) brain pressure at locations near the initial point of contact of the blast wave with the head, (2) displacement of the head, and (3) maximum principal strain in the brain tissue and the cerebral vasculature. Hence, we postulate that blast exposure at different animal orientations results in different biomechanical responses, which, in turn, lead to different alterations in the expression level of brain-tissue molecules and, potentially, different likelihood of brain injury. In fact, in a very recent study, Heyburn et al. reported differences in protein-expression levels in the brain of male Sprague-Dawley rats exposed to blast waves of 90, 110, and 130 kPa in a prone orientation with the head facing the blast wave versus those exposed to a blast wave at the same BOP in a side-on orientation [8]. They argue that the observed variations in protein-expression levels are due to differences in lung injury and to structural differences of the head that could have caused localized changes in stress and strain in the brain.

In addition to the animal orientation, displacement of the head can influence the response of brain tissue to blast-wave exposure. For example, Sawyer et al. showed that the displacement of the head of adult male Sprague-Dawley rats during blast exposure in a shock tube influences protein-expression levels in the brain [11]. They reported that restraining the head during blast exposure reduces the expression of glial fibrillary acidic protein in the cortex, hippocampus, cerebellum, and brainstem. It is well established that violent motion, either due to improper placement of animals within a shock tube or from end-jet testing (i.e., placement of animals outside of a shock tube), can unintentionally cause brain injury as an artifact of testing animals in shock tubes [21,37,38]. Our predictions of displacement of the rat head

demonstrate that the prone orientation (displacement of 2 mm) is preferable to the vertical (10 mm) and head-only (7 mm) orientations in order to minimize animal movement during experiments. While we did not measure displacement of the animal head during the blast experiments, using a similar setup and the same exact shock tube as in our study, Sawyer et al. [11] tracked the head motion at the eyes and nose of a rat during side-on, head-only exposures at a blast overpressure of 172 kPa, and reported displacements ranging between ~12 and 24 mm. When compared to our predictions, their reported values are slightly higher, which are possibly due to the higher blast overpressure, differences in animal restraint, and differences in head orientation relative to the direction of the blast wave.

Our study has limitations. First, to reduce computational time, we did not include the internal organs of the torso in the FE model. However, exclusion of these organs is unlikely to have influenced our pressure and strain predictions because the propagation of the pressure wave from the torso to the head was negligible. In addition, we did not represent the cerebrospinal fluid because we lacked its 3D geometry. This simplification may influence our predictions of brain strain. Second, as in our previous model [28], we coupled the rat brain with the cerebral vasculature using the embedded-element technique to avoid explicitly representing the vasculature in the model, as this requires the use of a large number of extremely small elements. The presence of extremely small elements in our model can cause numerical singularities in the FE meshes during blast simulations, which may lead to convergence issues. Moreover, while it is known that the embedded-element technique increases the mass in the FE model due to volume redundancy [39], we believe that, as the stiffness of the embedded material is orders of magnitude larger than the host material, the contribution of the excess mass to the stress distribution can be neglected [40]. Third, given the challenge of simultaneously measuring intracranial pressure in multiple locations across the brain, we validated our model by measuring pressure at only one location in the brain (i.e., at the right lateral ventricle). Moreover, due to the lack of experimental data on brain displacement and brain strain, we were unable to validate our computational model for strain predictions. In fact, experimental measurements of brain displacement during blast exposure in a shock tube on animals, cadavers, or even surrogate heads do not exist. Therefore, while we validated our pressure predictions at the ventricle for each of the three orientations, our predictions of head motion and brain strain could not be validated, or even qualitatively compared, due to the lack of experimental data. Fourth, we performed our study for an incident BOP of 100 kPa. However, we believe the influence of orientation on the brain responses observed in our study will remain valid for other BOPs that mimic mild TBI in a rat brain in shock tubes similar to the ABS. Finally, we performed all of our simulations for a duration of 5 ms and, similar to other FE simulations using ABAQUS [28,34], did not represent negative blast pressure. While a negative pressure can influence both the biomechanical responses of the brain tissue and the cerebral vasculature, we believe that the results of our comparative analyses would not have been different had we performed simulations beyond 5 ms or included negative pressures.

5 Conclusions

In summary, we systematically investigated the effect of animal orientation with respect to the direction of blast-wave propagation on the biomechanical responses of the rat brain during exposure to a blast wave in a shock tube. Our study shows that, for a given BOP, the orientation of the animal influences the forces acting on the animal, which depend on multiple factors, such as the surface area and angle of incidence of the blast wave. These forces, in turn, affect the biomechanical responses of brain tissues, such as pressure, von Mises stress, and strain, which can lead to orientation-dependent injury patterns in rat-brain tissues. These results show that we cannot make a direct comparison between the injury patterns obtained from different animal orientations, even for an identical BOP. Our study also highlights how a single brain-pressure measurement (often at the ventricle) cannot capture the effects of animal orientation on biomechanical responses. The predictions of our high-fidelity FE model will ultimately aid in identifying the mechanisms of blast-induced brain injury by determining region-specific correlates between biomechanical responses and brain-tissue changes due to blast exposure.

References

[1] Ahlers, S., Vasserman-Stokes, E., Shaughness, M., Hall, A., Shear, D., Chavko, M., McCarron, R., and Stone, J., 2012, "Assessment of the Effects of Acute and Repeated Exposure to Blast Overpressure in Rodents: Toward a Greater Understanding of Blast and the Potential Ramifications for Injury in Humans Exposed to Blast," Front. Neurol., **3**(32), pp. 1–12.

[2] Arun, P., Wilder, D. M., Eken, O., Urioste, R., Batuure, A., Sajja, S., Albert, S. V., Wang, Y., Gist, I. D., and Long, J. B., 2020, "Long-Term Effects of Blast Exposure: A Functional Study in Rats Using an Advanced Blast Simulator," J. Neurotrauma, **37**(4), pp. 647–655.

[3] Bolander, R., Mathie, B., Bir, C., Ritzel, D., and VandeVord, P., 2011, "Skull Flexure as a Contributing Factor in the Mechanism of Injury in the Rat When Exposed to a Shock Wave," Ann. Biomed. Eng., **39**(10), pp. 2550–2559.

[4] Chafi, M. S., Karami, G., and Ziejewski, M., 2010, "Biomechanical Assessment of Brain Dynamic Responses Due to Blast Pressure Waves," Ann. Biomed. Eng., **38**(2), pp. 490–504.

[5] Chavko, M., Watanabe, T., Adeeb, S., Lankasky, J., Ahlers, S. T., and McCarron, R. M., 2011, "Relationship Between Orientation to a Blast and Pressure Wave Propagation Inside the Rat Brain," J. Neurosci. Methods, **195**(1), pp. 61–66.

[6] Feng, K., Zhang, L., Jin, X., Chen, C., Kallakuri, S., Saif, T., Cavanaugh, J., and King, A., 2016, "Biomechanical Responses of the Brain in Swine Subject to Free-Field Blasts," Front. Neurol., **7**(179), pp. 1–12.

[7] Garman, R. H., Jenkins, L. W., Switzer, R. C., 3rd, Bauman, R. A., Tong, L. C., Swauger, P. V., Parks, S. A., Ritzel, D. V., Dixon, C. E., Clark, R. S., Bayir, H., Kagan, V., Jackson, E. K., and Kochanek, P. M., 2011, "Blast Exposure in Rats With Body Shielding is Characterized Primarily by Diffuse Axonal Injury," J. Neurotrauma, **28**(6), pp. 947–959.

[8] Heyburn, L., Abutarboush, R., Goodrich, S., Urioste, R., Batuure, A., Statz, J., Wilder, D., Ahlers, S. T., Long, J. B., and Sajja, V., 2019, "Repeated Low-Level Blast Overpressure Leads to Endovascular Disruption and Alterations in TDP-43 and Piezo2 in a Rat Model of Blast TBI," Front. Neurol., **10**(766), pp. 1–10.

[9] Leonardi, A., Keane, N. J., Bir, C. A., Ryan, A. G., Xu, L., and Vandevord, P. J., 2012, "Head Orientation Affects the Intracranial Pressure Response Resulting From Shock Wave Loading in the Rat," J. Biomech., **45**(15), pp. 2595–2602.

[10] Long, J. B., Bentley, T. L., Wessner, K. A., Cerone, C., Sweeney, S., and Bauman, R. A., 2009, "Blast Overpressure in Rats: Recreating a Battlefield Injury in the Laboratory," J. Neurotrauma, **26**(6), pp. 827–840.

[11] Sawyer, T. W., Wang, Y., Ritzel, D. V., Josey, T., Villanueva, M., Shei, Y., Nelson, P., Hennes, G., Weiss, J., Vair, C., Fan, C., and Barnes, J., 2016, "High-Fidelity Simulation of Primary Blast: Direct Effects on the Head," J. Neurotrauma, **33**(13), pp. 1181–1193.

[12] Skotak, M., Wang, F., Alai, A., Holmberg, A., Harris, S., Switzer, R. C., and Chandra, N., 2013, "Rat Injury Model Under Controlled Field-Relevant

Primary Blast Conditions: Acute Response to a Wide Range of Peak Overpressures," J. Neurotrauma, **30**(13), pp. 1147–1160.

[13] Sosa, M. A., De Gasperi, R., Paulino, A. J., Pricop, P. E., Shaughness, M. C., Maudlin-Jeronimo, E., Hall, A. A., Janssen, W. G., Yuk, F. J., Dorr, N. P., Dickstein, D. L., McCarron, R. M., Chavko, M., Hof, P. R., Ahlers, S. T., and Elder, G. A., 2013, "Blast Overpressure Induces Shear-Related Injuries in the Brain of Rats Exposed to a Mild Traumatic Brain Injury," Acta Neuropathol. Commun., **1**(1), p. 15.

[14] Cernak, I., 2010, "The Importance of Systemic Response in the Pathobiology of Blast-Induced Neurotrauma," Front. Neurol., **1**(151), pp. 1–9.

[15] Kuriakose, M., Rama Rao, K. V., Younger, D., and Chandra, N., 2018, "Temporal and Spatial Effects of Blast Overpressure on Blood-Brain Barrier Permeability in Traumatic Brain Injury," Sci. Rep., **8**(1), pp. 1–14.

[16] Bryden, D. W., Tilghman, J. I., and Hinds, S. R., 2019, "Blast-Related Traumatic Brain Injury: Current Concepts and Research Considerations," J. Exp. Neurosci., **13**, pp. 1–11.

[17] Hicks, R. R., Fertig, S. J., Desrocher, R. E., Koroshetz, W. J., and Pancrazio, J. J., 2010, "Neurological Effects of Blast Injury," J. Trauma, **68**(5), pp. 1257–1263.

[18] Risling, M., Plantman, S., Angeria, M., Rostami, E., Bellander, B. M., Kirkegaard, M., Arborelius, U., and Davidsson, J., 2011, "Mechanisms of Blast Induced Brain Injuries, Experimental Studies in Rats," NeuroImage, **54**, pp. S89–S97.

[19] Rodriguez, U. A., Zeng, Y., Deyo, D., Parsley, M. A., Hawkins, B. E., Prough, D. S., and DeWitt, D. S., 2018, "Effects of Mild Blast Traumatic Brain Injury on Cerebral Vascular, Histopathological, and Behavioral Outcomes in Rats," J. Neurotrauma, **35**(2), pp. 375–392.

[20] Sajja, V. S. S. S., Hubbard, W. B., Hall, C. S., Ghoddoussi, F., Galloway, M. P., and VandeVord, P. J., 2015, "Enduring Deficits in Memory and Neuronal Pathology After Blast-Induced Traumatic Brain Injury," Sci. Rep., **5**(1), pp. 1–10.

[21] Sundaramurthy, A., Alai, A., Ganpule, S., Holmberg, A., Plougonven, E., and Chandra, N., 2012, "Blast-Induced Biomechanical Loading of the Rat: An Experimental and Anatomically Accurate Computational Blast Injury Model," J. Neurotrauma, **29**(13), pp. 2352–2364.

[22] Sajja, V. S., Arun, P., Van Albert, S. A., and Long, J. B., 2018, "Rodent Model of Primary Blast-Induced Traumatic Brain Injury: Guidelines to Blast Methodology," *Pre-Clinical and Clinical Methods in Brain Trauma Research*, A. K. Srivastava and C. S. Cox, eds., Springer, New York, pp. 123–138.

[23] Kovesdi, E., Kamnaksh, A., Wingo, D., Ahmed, F., Grunberg, N., Long, J., Kasper, C., and Agoston, D., 2012, "Acute Minocycline Treatment Mitigates the Symptoms of Mild Blast-Induced Traumatic Brain Injury," Front. Neurol., **3**(111), pp. 1–18.

[24] Kwon, S.-K., Kovesdi, E., Gyorgy, A., Wingo, D., Kamnaksh, A., Walker, J., Long, J., and Agoston, D., 2011, "Stress and Traumatic Brain Injury: A Behavioral, Proteomics, and Histological Study," Front. Neurol., **2**(12), pp. 1–14.

[25] Abutarboush, R., Gu, M., Kawoos, U., Mullah, S. H., Chen, Y., Goodrich, S. Y., Lashof-Sullivan, M., McCarron, R. M., Statz, J. K., Bell, R. S., Stone, J. R., and Ahlers, S. T., 2019, "Exposure to Blast Overpressure Impairs Cerebral Microvascular Responses and Alters Vascular and Astrocytic Structure," J. Neurotrauma, **36**(22), pp. 3138–3157.

[26] Hubbard, W. B., Greenberg, S., Norris, C., Eck, J., Lavik, E., and VandeVord, P., 2017, "Distinguishing the Unique Neuropathological Profile of Blast Polytrauma," Oxid. Med. Cell. Longevity, **2017**(5175249), pp. 1–11.

[27] Kochanek, P. M., Dixon, C. E., Shellington, D. K., Shin, S. S., Bayır, H., Jackson, E. K., Kagan, V. E., Yan, H. Q., Swauger, P. V., Parks, S. A., Ritzel, D. V., Bauman, R., Clark, R. S. B., Garman, R. H., Bandak, F., Ling, G., and Jenkins, L. W., 2013, "Screening of Biochemical and Molecular Mechanisms of Secondary Injury and Repair in the Brain After Experimental Blast-Induced Traumatic Brain Injury in Rats," J. Neurotrauma, **30**(11), pp. 920–937.

[28] Unnikrishnan, G., Mao, H., Sundaramurthy, A., Bell, E. D., Yeoh, S., Monson, K., and Reifman, J., 2019, "A 3-D Rat Brain Model for Blast-Wave Exposure: Effects of Brain Vasculature and Material Properties," Ann. Biomed. Eng., **47**(9), pp. 2033–2044.

[29] Keenan, M. A., Stabin, M. G., Segars, W. P., and Fernald, M. J., 2010, "RADAR Realistic Animal Model Series for Dose Assessment," J. Nucl. Med., **51**(3), pp. 471–476.

[30] Rakesh, V., Stallings, J. D., Helwig, B. G., Leon, L. R., Jackson, D. A., and Reifman, J., 2013, "A 3-D Mathematical Model to Identify Organ-Specific Risks in Rats During Thermal Stress," J. Appl. Physiol., **115**(12), pp. 1822–1837.

[31] Rakesh, V., Stallings, J. D., and Reifman, J., 2014, "A Virtual Rat for Simulating Environmental and Exertional Heat Stress," J. Appl. Physiol., **117**(11), pp. 1278–1286.

[32] Haslach, H. W., Gipple, J. M., and Leahy, L. N., 2017, "Influence of High Deformation Rate, Brain Region, Transverse Compression, and Specimen Size on Rat Brain Shear Stress Morphology and Magnitude," J. Mech. Behav. Biomed. Mater., **68**, pp. 88–102.

[33] Bell, D., Converse, M., Mao, H., Unnikrishnan, G., Reifman, J., and Monson, K., 2018, "Material Properties of Rat Middle Cerebral Arteries at High Strain Rates," ASME J. Biomech. Eng., **140**(7), p. 071004.

[34] Sundaramurthy, A., Skotak, M., Alay, E., Unnikrishnan, G., Mao, H., Duan, X., Williams, S. T., Harding, T. H., Chandra, N., and Reifman, J., 2018, "Assessment of the Effectiveness of Combat Eyewear Protection Against Blast Overpressure," ASME J. Biomech. Eng., **140**(7), p. 071003.

[35] Bir, C., Bolander, R., Leonardi, A., Ritzel, D., VandeVord, P., and Dingell, J., 2011, "A Biomechanical Prospective of Blast Injury Neurotrauma," Proceedings of the HFM 207 NATO Symposium on a Survey of Blast Injury Across the Full Landscape of Military Science, Halifax, NS, Canada, Oct. 17, Paper No. MP-HFM-207-27.

[36] Panzer, M. B., Myers, B. S., and Bass, C. R., 2013, "Mesh Considerations for Finite Element Blast Modelling in Biomechanics," Comput. Methods Biomech. Biomed. Eng., **16**(6), pp. 612–621.

[37] Kahali, S., Townsend, H., Mendez Nguyen, M., Kim, J., Alay, E., Skotak, M., and Chandra, N., 2020, "The Evolution of Secondary Flow Phenomena and Their Effect on Primary Shock Conditions in Shock Tubes: Experimentation and Numerical Model," PLoS One, **15**(1), p. e0227125.

[38] Needham, C. E., Ritzel, D., Rule, G. T., Wiri, S., and Young, L., 2015, "Blast Testing Issues and TBI: Experimental Models That Lead to Wrong Conclusions," Front. Neurol., **6**(72), pp. 1–10.

[39] Garimella, H. T., and Kraft, R. H., 2017, "Modeling the Mechanics of Axonal Fiber Tracts Using the Embedded Finite Element Method," Int. J. Numer. Methods Biomed. Eng., **33**(5), p. e2823.

[40] Matveeva, A. V., Romanov, S., Lomov, and Gorbatikh, L., 2015, "Application of the Embedded Element Technique to the Modelling of Nano-Engineered Fiber-Reinforced Composites," 20th International Conference on Composite Materials, Copenhagen, Denmark, July 19–24, Paper No. 2102–2.